Journal of Power Sources 265 (2014) 174–181

Contents lists available at ScienceDirect

Journal of Power Sources

journal homepage: www.elsevier.com/locate/jpowsour

Design, synthesis, and performances of double-shelled $LiNi_{0.5}Co_{0.2}Mn_{0.3}O_2$ as cathode for long-life and safe Li-ion battery

Peiyu Hou [a], Xiaoqing Wang [b], Dawei Song [a,*], Xixi Shi [a], Lianqi Zhang [a,**], Jian Guo [c], Jun Zhang [c]

[a] School of Materials Science and Engineering, Tianjin University of Technology, Tianjin 300384, China
[b] School of Environment and Chemical Engineering, Tianjin Polytechnic University, Tianjin 300387, China
[c] Pylon Technologies Co., Ltd, Shanghai 201203, China

HIGHLIGHTS

- $LiNi_{0.5}Co_{0.2}Mn_{0.3}O_2$ is designed to double-shelled structure.
- Double-shelled material exhibits improved cycleability and thermal stability.
- Double-shelled sample displays more excellent rate capability.
- The improved performances are probably attributed to the stable and porous outer shell.

ARTICLE INFO

Article history:
Received 28 December 2013
Received in revised form
7 April 2014
Accepted 22 April 2014
Available online 2 May 2014

Keywords:
Cathode materials
$LiNi_{0.5}Co_{0.2}Mn_{0.3}O_2$
Double-shelled structure
Co-precipitation
Li-ion battery

ABSTRACT

$LiNi_{0.5}Co_{0.2}Mn_{0.3}O_2$ is redesigned into a new core-shelled $Li[(Ni_{0.8}Co_{0.1}Mn_{0.1})_{2/7}]_{core}[(Ni_{1/3}Co_{1/3}Mn_{1/3})_{3/14}]_{inner\text{-}shell}[(Ni_{0.4}Co_{0.2}Mn_{0.4})_{1/2}]_{outer\text{-}shell}O_2$, in which $LiNi_{0.8}Co_{0.1}Mn_{0.1}O_2$ may deliver high capacity and $LiNi_{0.4}Co_{0.2}Mn_{0.4}O_2$ provides structural and thermal stability. To achieve such designed structure, double-shelled hydroxide precursors are firstly prepared via a co-precipitation route. Scanning electron microscope (SEM) shows that all precursors are of 6–10 μm spherical secondary particles developed from nanosheet-shaped primary particles. Energy disperse X-ray spectrum (EDS) on the surface of precursors, in combination with increase of particles size from core to shell during co-precipitation process, confirms the formation of core–shell structure as designed. The spherical morphology is preserved after lithiation at different temperatures from 800 °C to 900 °C while the morphology of primary particles changes from nano-sized plate to micron-sized rectangular-like shapes. EDS surface composition analysis of lithiated compounds also strongly suggests the formation of core–shell structure; nevertheless, diffusion of transition metal ions between the core and shell occurs and becomes severe with increase of sintering temperature. Consequently, the double-shelled materials especially prepared at 850 °C display the remarkably improved cycleability, rate capability, and thermal stability in contrast to normal one. The enhancement of those properties may be ascribed to structurally stable double shell components, especially outer shell.

1. Introduction

$LiCoO_2$ has been widely used as the commercial cathode material for lithium ion batteries [1]. However, it also has some limitations such as toxicity, high cost and instability at high voltages (above 4.3 V) [2,3], which has led to study of other candidate cathode materials. $LiNi_{1-x-y}Co_xMn_yO_2$ has been considered as an alternative cathode material to replace $LiCoO_2$ [4–13]. Among the potential materials, $LiNi_{0.5}Co_{0.2}Mn_{0.3}O_2$ is considered as one of the most promising materials in respect to its lower cost, less toxicity, and larger reversible capacity [14–16]. Further enhancement of its cycleability and safety properties is still required [17]. Various efforts such as using different synthesis methods and lithium sources

* Corresponding author. Tel.: +86 22 60214577; fax: +86 22 60214028.
** Corresponding author. Tel.: +86 22 60214578; fax: +86 22 60214028.
E-mail addresses: songdw2005@mail.nankai.edu.cn (D. Song), tianjinzhanglq@163.com (L. Zhang).

http://dx.doi.org/10.1016/j.jpowsour.2014.04.107
0378-7753/

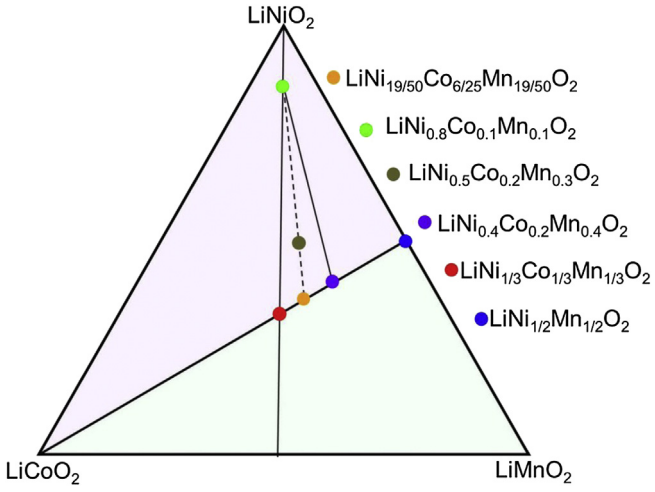

Fig. 1. The triangle phase diagram of $LiNiO_2$–$LiCoO_2$–$LiMnO_2$.

[18,19], surface modification were reported to solve the problems [20–22], but the gain is little.

Recently, construction of core–shell structures in layered $LiNi_{1-x-y}Co_xMn_yO_2$ by co-precipitation method was reported to be able to remarkably enhance the cycleability and safety property [23–26]. $Li[(Ni_{1/2}Mn_{1/2})_{1-x}Co_x]O_2$ ($x = 0$–$1/3$) are usually used as the shell in core–shell structures due to excellent cycling performance and thermal stability [4,6,27–31]. The valence of transition metal element is Ni(+2), Co(+3) and Mn(+4) in $Li[(Ni_{1/2}Mn_{1/2})_{1-x}Co_x]O_2$ [28–32]. In these compounds, the electrochemically inactive tetravalent Mn provides significant structural stability and results in a simple topotactic reaction maintaining the hexagonal phase during electrochemical cycling, even at a high voltage cutoff limit of 4.6 V [31–34]. Therefore, construction of core–shell structures in $LiNi_{0.5}Co_{0.2}Mn_{0.3}O_2$ to improve its performances without altering total compositions is of much interest and meanful from application. According to the reported core–shell layered $LiNi_{1-x-y}Co_xMn_yO_2$ materials, a basic rule for building the core–shell structure is that core and shell component materials should have the similar layered structure and can form solid solution. Fig. 1 shows a triangle phase diagram of $LiNiO_2$–$LiCoO_2$–$LiMnO_2$. According to our knowledge of references [35], the compositions on the joint line of $LiCoO_2$–$LiNi_{1/2}Mn_{1/2}O_2$ in the triangle phase diagram of $LiNiO_2$–$LiCoO_2$–$LiMnO_2$ can form $LiNi_zCo_{1-2z}Mn_zO_2$ solid solution and is also the border between pure phase and impure phase regions in the phase diagram. The pure phase (solid solution) can form in the region of $LiNiO_2$–$LiCoO_2$–$LiNi_{1/2}Mn_{1/2}O_2$ and cannot usually be obtained via a conventional high-temperature solid state reaction in the region of $LiMnO_2$–$LiCoO_2$–$LiNi_{1/2}Mn_{1/2}O_2$. $LiNi_{0.5}Co_{0.2}Mn_{0.3}O_2$ in the pure phase region can be decomposed into various components according to the phase diagram. If $LiNi_{0.8}Co_{0.1}Mn_{0.1}O_2$ having a high capacity is chosen as core component [36] and $LiNi_{0.4}Co_{0.2}Mn_{0.4}O_2$ having good structural stability [27] as shell component, another composition as a transitional layer is needed to form the composition of $LiNi_{0.5}Co_{0.2}Mn_{0.3}O_2$. $LiNi_{1/3}Co_{1/3}Mn_{1/3}O_2$ can be selected as a transitional composition layer according to the phase diagram. Therefore, $LiNi_{0.5}Co_{0.2}Mn_{0.3}O_2$ can finally be redesigned into a new core-shelled $Li[(Ni_{0.8}Co_{0.1}Mn_{0.1})_{2/7}]_{core}[(Ni_{1/3}Co_{1/3}Mn_{1/3})_{3/14}]_{inner\text{-}shell}[(Ni_{0.4}Co_{0.2}Mn_{0.4})_{1/2}]_{outer\text{-}shell}O_2$ structure. In addition, selection of $LiNi_{0.4}Co_{0.2}Mn_{0.4}O_2$ and $LiNi_{1/3}Co_{1/3}Mn_{1/3}O_2$ as shells is also in view of their good processing property of electrode as well as their mature synthesis route, which may probably improve processing property of $LiNi_{0.5}Co_{0.2}Mn_{0.3}O_2$ electrode.

In this work, a double-shelled $Li[(Ni_{0.8}Co_{0.1}Mn_{0.1})_{2/7}]_{core}[(Ni_{1/3}Co_{1/3}Mn_{1/3})_{3/14}]_{inner\text{-}shell}[(Ni_{0.4}Co_{0.2}Mn_{0.4})_{1/2}]_{outer\text{-}shell}O_2$, which has the same composition as $LiNi_{0.5}Co_{0.2}Mn_{0.3}O_2$, was proposed and synthesized via a co-precipitation route to improve performances of $LiNi_{0.5}Co_{0.2}Mn_{0.3}O_2$. Furthermore, lithium carbonate

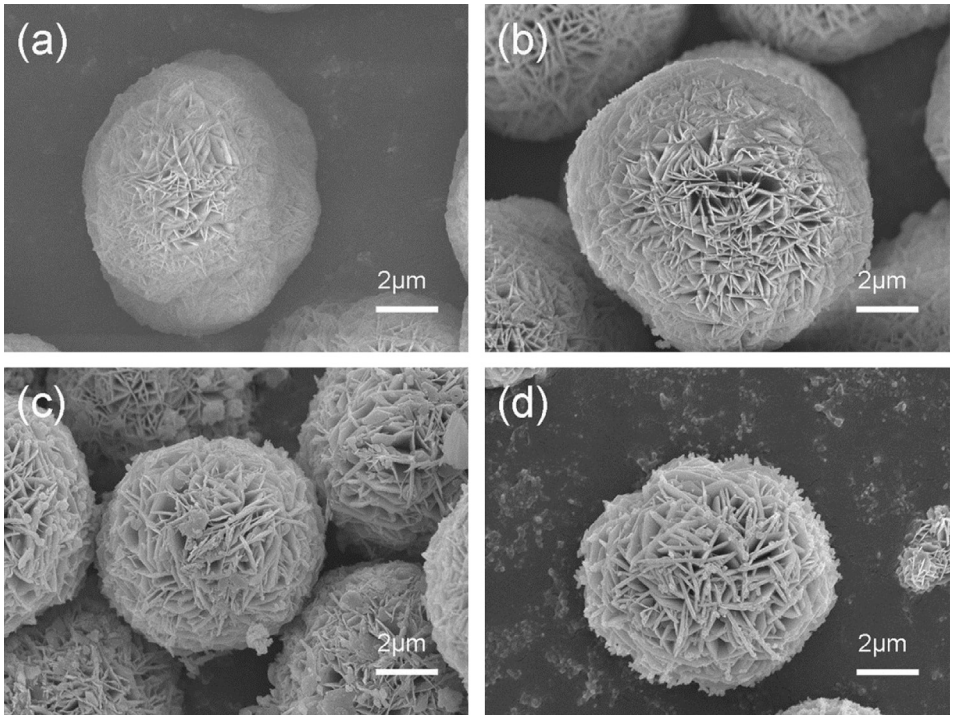

Fig. 2. SEM images of precursors (a) core $[Ni_{0.8}Co_{0.1}Mn_{0.1}](OH)_2$, (b) one-shelled $[(Ni_{0.8}Co_{0.1}Mn_{0.1})_{4/7}(Ni_{1/3}Co_{1/3}Mn_{1/3})_{3/7}](OH)_2$, (c) double-shelled $[(Ni_{0.8}Co_{0.1}Mn_{0.1})_{2/7}(Ni_{1/3}Co_{1/3}Mn_{1/3})_{3/14}(Ni_{0.4}Co_{0.2}Mn_{0.4})_{1/2}](OH)_2$ and (d) normal $[Ni_{0.5}Co_{0.2}Mn_{0.3}](OH)_2$.

Table 1
Total chemical compositions of Ni, Co and Mn elements in molar ratio obtained from ICP analysis for normal and double-shelled $[Ni_{0.5}Co_{0.2}Mn_{0.3}](OH)_2$ precursors.

	Observed molar ratio			Aimed molar ratio		
	Ni	Co	Mn	Ni	Co	Mn
Normal precursors	0.496	0.199	0.305	0.5	0.2	0.3
Double shelled precursors	0.497	0.201	0.302			

instead of lithium hydroxide in this work was used as lithium source in comparison with previously reported core-shelled compounds [24]. The comparative investigation between double-shelled and normal $LiNi_{0.5}Co_{0.2}Mn_{0.3}O_2$ materials was performed in detail.

2. Experimental

To synthesize the spherical core $[Ni_{0.8}Co_{0.1}Mn_{0.1}](OH)_2$ precursors, stoichiometric $NiSO_4 \cdot 6H_2O$, $CoSO_4 \cdot 7H_2O$ and $MnSO_4 \cdot H_2O$ were dissolved with a concentration of 2.5 mol L^{-1} as the core solution (aq). Then the core solution of sulfates (14.29 L) and a mixed aqueous alkaline solution (aq) with 10 mol L^{-1} NaOH as the pH control agent and 1.5 mol L^{-1} NH_4OH as the chelating agent, were simultaneously pumped into a continuously stirred tank reactor (CSTR, capacity of 170 L) under a nitrogen atmosphere to react at 50 °C by automatically controlling a constant pH value of about 11 and keeping a stirring rate of 500 rpm. The complete consumption of the core sulfate solution finally led to the core $[Ni_{0.8}Co_{0.1}Mn_{0.1}](OH)_2$ precursors. Subsequently, the aqueous first-layer shell solution (cationic ratio of Ni:Co:Mn = 1:1:1, 10.71 L) in place of core sulfates solution was continuously pumped into the reactor to encapsulate the core under a constant pH (10.6). The complete consumption of the first-shell sulfate solution resulted in one-shelled $[(Ni_{0.8}Co_{0.1}Mn_{0.1})_{4/7}(Ni_{1/3}Co_{1/3}Mn_{1/3})_{3/7}](OH)_2$ precursor. Finally, the second-layer shell sulfate solution (25.0 L, cationic ratio of Ni:Co:Mn = 2:1:2) was further continuously pumped into the reactor under a constant pH (10.6), leading to double-shelled $([(Ni_{0.8}Co_{0.1}Mn_{0.1})_{2/7}(Ni_{1/3}Co_{1/3}Mn_{1/3})_{3/14}(Ni_{0.4}Co_{0.2}Mn_{0.4})_{1/2}](OH)_2$ precursor. The velocity for pumping sulfate solutions into the reactor is about 1.5 L per hour, and thus the total reaction time is about 33 h. The normal $[Ni_{0.5}Co_{0.2}Mn_{0.3}](OH)_2$ precursors were also synthesized via a similar co-precipitation route.

The obtained hydroxide precursors were filtered, washed, and dried for 24 h in air. The mixture of the obtained precursors with a stoichiometric ratio Li_2CO_3 powder was preheated to 750 °C for 4 h and subsequently calcined at 800 °C, 850 °C, and 900 °C for 16 h in a furnace under air to form lithiated materials, respectively.

Table 2
Surface compositions of Ni, Co and Mn elements in molar ratio obtained from EDS experiments for core, one-shelled, double-shelled and normal precursors.

	Observed molar ratio			Aimed molar ratio		
	Ni	Co	Mn	Ni	Co	Mn
Normal precursors $[Ni_{0.5}Co_{0.2}Mn_{0.3}](OH)_2$	0.503	0.191	0.306	0.5	0.2	0.3
Core precursors $[Ni_{0.8}Co_{0.1}Mn_{0.1}](OH)_2$	0.796	0.103	0.101	0.8	0.1	0.1
One-shelled precursors $[(Ni_{0.8}Co_{0.1}Mn_{0.1})_{4/7}(Ni_{1/3}Co_{1/3}Mn_{1/3})_{3/7}](OH)_2$	0.333	0.334	0.332	0.333	0.333	0.333
Double-shelled precursors $[(Ni_{0.8}Co_{0.1}Mn_{0.1})_{2/7}(Ni_{1/3}Co_{1/3}Mn_{1/3})_{3/14}(Ni_{0.4}Co_{0.2}Mn_{0.4})_{1/2}](OH)_2$	0.392	0.206	0.402	0.4	0.2	0.4

Precursors products were periodically collected every two hours during the co-precipitation experiment for monitoring the growth conditions of precursors particle size. And the particle size distribution was measured with a particle size analyzer (OMEC, LS-POP(6), China). X-ray diffractometry (XRD, Rigaku D/MAX-2500 Japan) was employed to characterize structure of the prepared materials. The morphology of synthesized materials was observed by a scanning electron microscope (SEM, JMS-6700F, JEOL, Japan). Energy dispersive X-ray spectroscopy (EDS, Hiroba EDX) was used to analyze surface chemical composition of precursors and lithiated materials. The total chemical compositions of precursors were analyzed by an inductively coupled plasmas spectrometer (ICP, SPS 7800, Seiko Instruments, Japan). The specific surface area of the samples was determined by N_2 adsorption using a 3H-2000 specific surface area instrument (Brunauer Emmett Teller, BET).

For differential scanning calorimetry (DSC) experiments, cells were finally charged to 4.3 V and opened carefully in the Ar-filled dry box. After opening the cells, the electrode materials were recovered from the current collector. The DSC data were collected in a DSC (NETZSCH 204F1,Germany) using a temperature scan rate of 4 °C min^{-1} in the temperature range of 50–350 °C.

For fabrication of cathode electrodes, the prepared materials were mixed with acetylene black and PVDF (83:10:7 in weight) in *N*-methyl-2-pyrrolidone. The obtained slurry was coated onto Al foil and dried at 80 °C for a day, followed by a roll-pressing. Prior to use, the electrodes were dried again at 120 °C for half a day in a vacuum oven. The electrodes were electrochemically characterized using a 2032 type of coin cell with lithium foil as the anode and 1 M $LiPF_6$ in ethylene carbonate diethyl carbonate (1:1 in volume) as the electrolyte. The cells were charged and discharged in the voltage range of 3.0–4.3 V (versus Li) under different conditions.

3. Results and discussion

Fig. 2 shows SEM images of the core precursor $[Ni_{0.8}Co_{0.1}Mn_{0.1}](OH)_2$, one-shelled precursor $[(Ni_{0.8}Co_{0.1}Mn_{0.1})_{4/7}(Ni_{1/3}Co_{1/3}Mn_{1/3})_{3/7}](OH)_2$, double-shelled precursor $[(Ni_{0.8}Co_{0.1}Mn_{0.1})_{2/7}(Ni_{1/3}Co_{1/3}Mn_{1/3})_{3/14}(Ni_{0.4}Co_{0.2}Mn_{0.4})_{1/2}](OH)_2$, and normal precursor $[Ni_{0.5}Co_{0.2}Mn_{0.3}](OH)_2$, respectively. All precursors are of

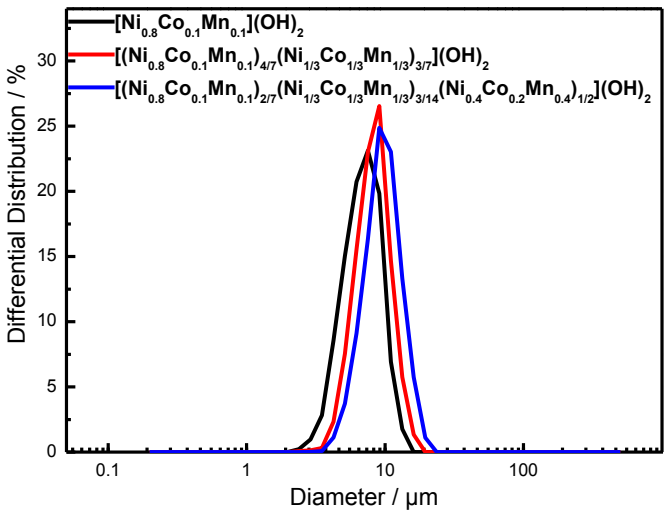

Fig. 3. The change in particle size distribution of double-shelled $[(Ni_{0.8}Co_{0.1}Mn_{0.1})_{2/7}(Ni_{1/3}Co_{1/3}Mn_{1/3})_{3/14}(Ni_{0.4}Co_{0.2}Mn_{0.4})_{1/2}](OH)_2$ precursors during the precipitation from core ($[Ni_{0.8}Co_{0.1}Mn_{0.1}](OH)_2$) to one-shelled ($[(Ni_{0.8}Co_{0.1}Mn_{0.1})_{4/7}(Ni_{1/3}Co_{1/3}Mn_{1/3})_{3/7}](OH)_2$) to double-shelled ($[(Ni_{0.8}Co_{0.1}Mn_{0.1})_{2/7}(Ni_{1/3}Co_{1/3}Mn_{1/3})_{3/14}(Ni_{0.4}Co_{0.2}Mn_{0.4})_{1/2}](OH)_2$) steps.

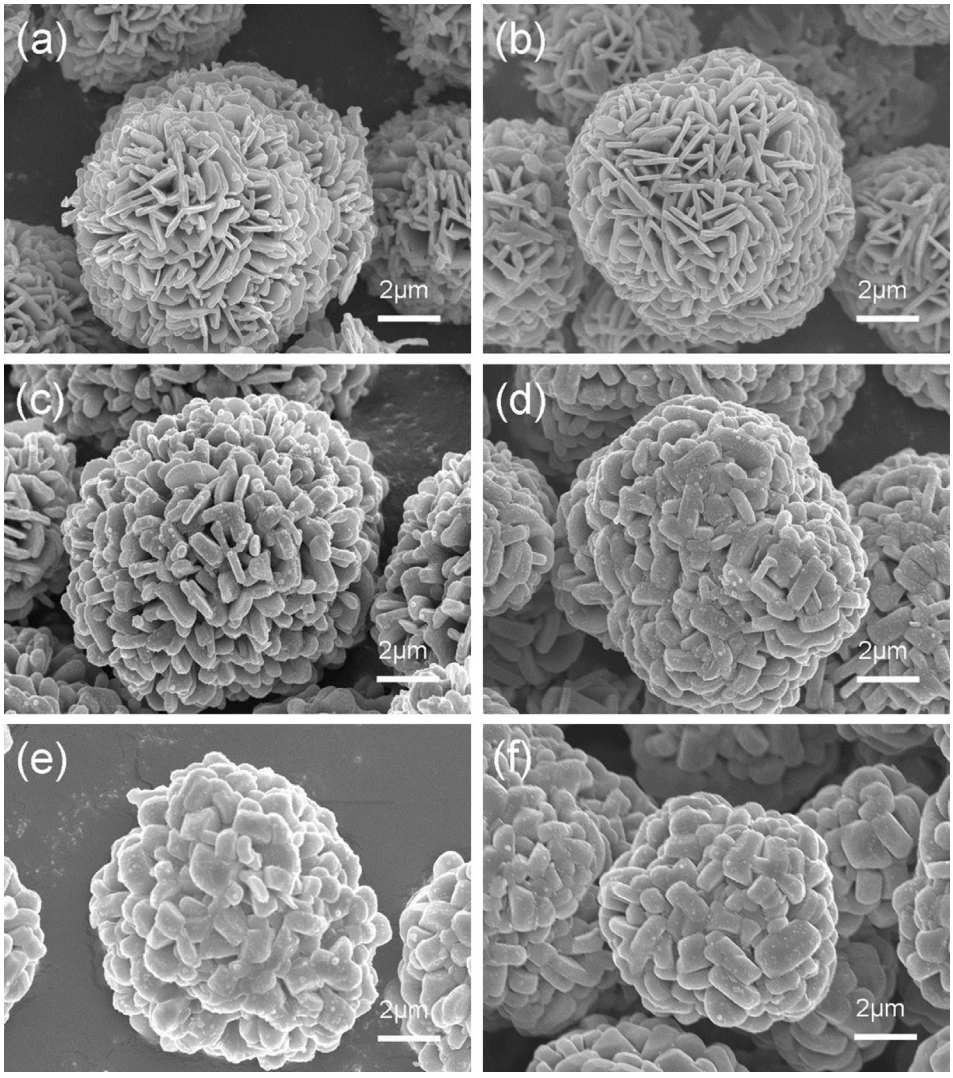

Fig. 4. SEM images of double-shelled $LiNi_{0.5}Co_{0.2}Mn_{0.3}O_2$ prepared at (a) 800 °C, (c) 850 °C, (e) 900 °C and normal $LiNi_{0.5}Co_{0.2}Mn_{0.3}O_2$ at (b) 800 °C, (d) 850 °C, (f) 900 °C.

spherical secondary particles with a large size of 6–10 μm, which are developed from plate-like primary particles with a nanosized thickness. The total chemical compositions of Ni, Co and Mn elements obtained by ICP for the normal precursor and double-shelled precursor $[Ni_{0.5}Co_{0.2}Mn_{0.3}](OH)_2$ are listed in Table 1. The total chemical compositions of normal and double-shelled precursors are $[Ni_{0.496}Co_{0.199}Mn_{0.305}](OH)_2$ and $[Ni_{0.497}Co_{0.201}Mn_{0.302}](OH)_2$, respectively, displaying quite good consistency with the targeted $[Ni_{0.5}Co_{0.2}Mn_{0.3}](OH)_2$. The surface chemical compositions of Ni, Co and Mn elements obtained from EDS experiments for core, one-shelled, double-shelled, and normal precursors are shown in Table 2. The detected surface chemical composition of core, one-shelled, double-shelled, and normal precursors are $[Ni_{0.796}Co_{0.103}Mn_{0.101}](OH)_2$, $[Ni_{0.333}Co_{0.334}Mn_{0.332}](OH)_2$,

Table 3
Surface compositions of Ni, Co and Mn elements in molar ratio obtained from EDS experiments for double-shelled $LiNi_{0.5}Co_{0.2}Mn_{0.3}O_2$ calcined at 800, 850 and 900 °C.

	Observed molar ratio			Aimed molar ratio		
	Ni	Co	Mn	Ni	Co	Mn
800 °C	0.403	0.194	0.403			
850 °C	0.416	0.201	0.383	0.4	0.2	0.4
900 °C	0.433	0.205	0.361			

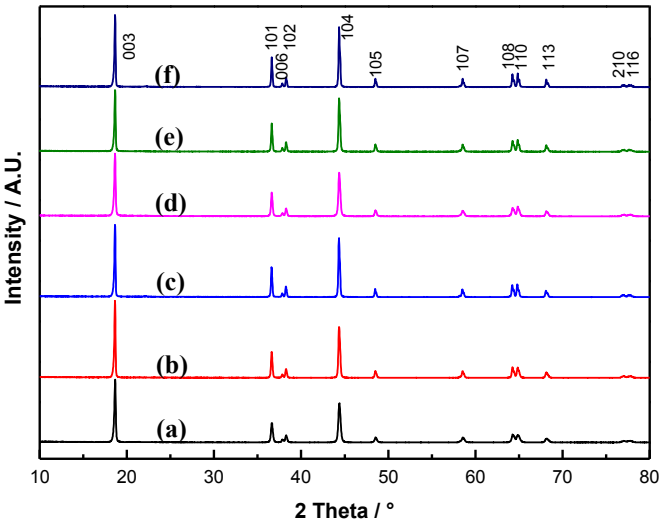

Fig. 5. XRD patterns of double-shelled $LiNi_{0.5}Co_{0.2}Mn_{0.3}O_2$ prepared at (a) 800 °C, (c) 850 °C, (e) 900 °C and normal $LiNi_{0.5}Co_{0.2}Mn_{0.3}O_2$ at (b) 800 °C, (d) 850 °C, (f) 900 °C.

Table 4
Comparison of lattice parameters of double-shelled and normal $LiNi_{0.5}Co_{0.2}Mn_{0.3}O_2$ prepared at different calcination temperatures.

	Lattice parameters	
	a/Å	*c*/Å
Double-shelled $LiNi_{0.5}Co_{0.2}Mn_{0.3}O_2$		
800 °C	2.8760	14.2631
850 °C	2.8759	14.2616
900 °C	2.8751	14.2604
Normal $LiNi_{0.5}Co_{0.2}Mn_{0.3}O_2$		
800 °C	2.8744	14.2542
850 °C	2.8732	14.2501
900 °C	2.8731	14.2478

Table 5
Comparison of initial charge–discharge capacities and efficiency for double-shelled and normal $LiNi_{0.5}Co_{0.2}Mn_{0.3}O_2$ prepared at different calcination temperatures.

	Charge capacity (mAh g^{-1})	Discharge capacity (mAh g^{-1})	Initial efficiency (%)
Double-shelled $LiNi_{0.5}Co_{0.2}Mn_{0.3}O_2$			
800 °C	200.1	166.2	83.1
850 °C	192.7	171.5	89.0
900 °C	193.0	162.5	84.2
Normal $LiNi_{0.5}Co_{0.2}Mn_{0.3}O_2$			
800 °C	195.7	163.9	83.7
850 °C	194.4	168.7	86.8
900 °C	200.0	169.2	84.6

$[Ni_{0.392}Co_{0.206}Mn_{0.402}](OH)_2$ and $[Ni_{0.503}Co_{0.191}Mn_{0.306}](OH)_2$, respectively, also showing good consistency with aimed ones. Therefore, the designed core–shell structures in precursors presumably are obtained successfully according to ICP and the surface EDS data as well as the reported core-shelled hydroxide precursors [24,37]. In addition, the generation of core–shell structures in precursors can also be well supported by the increase of the particle size from core to shell components during co-precipitation process. Fig. 3 shows the change in particle size distribution of double-shelled $[(Ni_{0.8}Co_{0.1}Mn_{0.1})_{2/7}(Ni_{1/3}Co_{1/3}Mn_{1/3})_{3/14}(Ni_{0.4}Co_{0.2}Mn_{0.4})_{1/2}](OH)_2$ precursors during the precipitation from core ($[Ni_{0.8}Co_{0.1}Mn_{0.1}](OH)_2$) to one-shelled ($[(Ni_{0.8}Co_{0.1}Mn_{0.1})_{4/7}(Ni_{1/3}Co_{1/3}Mn_{1/3})_{3/7}](OH)_2$) to double-shelled ($[(Ni_{0.8}Co_{0.1}Mn_{0.1})_{2/7}(Ni_{1/3}Co_{1/3}Mn_{1/3})_{3/14}(Ni_{0.4}Co_{0.2}Mn_{0.4})_{1/2}](OH)_2$) steps. All the curves have a single and narrow distribution peak. The formation of new crystal nuclei is not detected according to the particle size analysis every two hours during co-precipitation. Furthermore, as shell components are co-precipitated, particle size gradually increases. Therefore, it can be deduced that the shell components are co-precipitated onto the core part rather than generation of the new particle alone. The average particle diameters (D_{50}) of the core, one-shelled, and double-shelled precursors are 6.10 μm, 7.35 μm and to 8.63 μm, respectively, which suggests the thickness of inner-shell $[Ni_{1/3}Co_{1/3}Mn_{1/3}](OH)_2$ and outer-shell $[Ni_{0.4}Co_{0.2}Mn_{0.4}](OH)_2$ in double-shelled precursors are 0.625 μm and 0.64 μm, respectively.

The prepared precursors were calcined with a stoichiometric ratio of lithium carbonate at different temperatures from 800 °C to 900 °C. SEM (in Fig. 4) shows that the spherical morphology can be maintained well even after lithiation at high temperatures from 800 °C to 900 °C, but primary particles change from nanosized

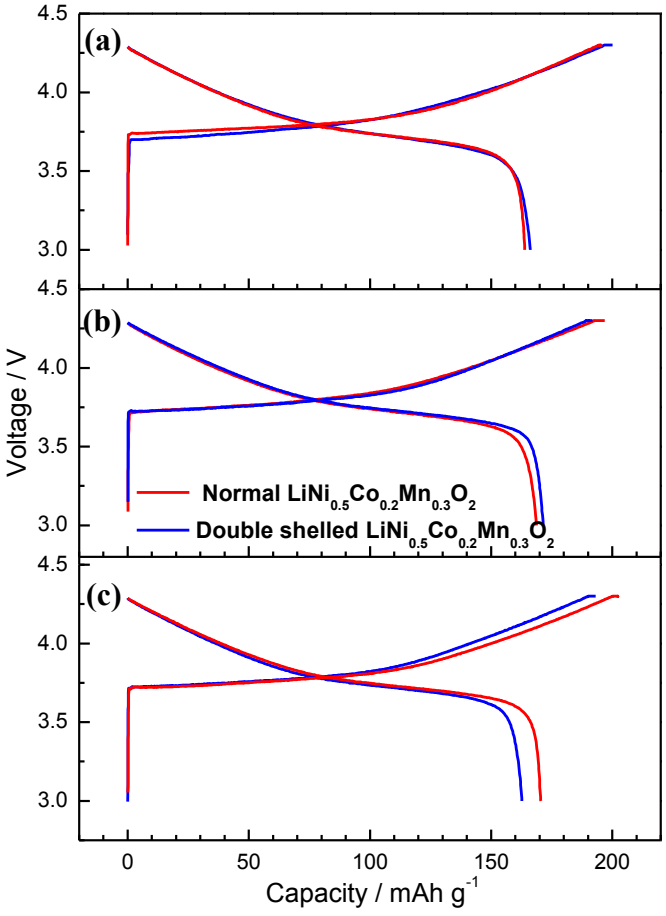

Fig. 6. The initial charge–discharge curves of normal and double-shelled $LiNi_{0.5}Co_{0.2}Mn_{0.3}O_2$ prepared at different temperatures in the voltage range of 3.0–4.3 V at 25 °C at a constant current density of 20 mA g^{-1} for initial three cycles and 150 mA g^{-1} for subsequent cycles: (a) 800 °C, (b) 850 °C, (c) 900 °C.

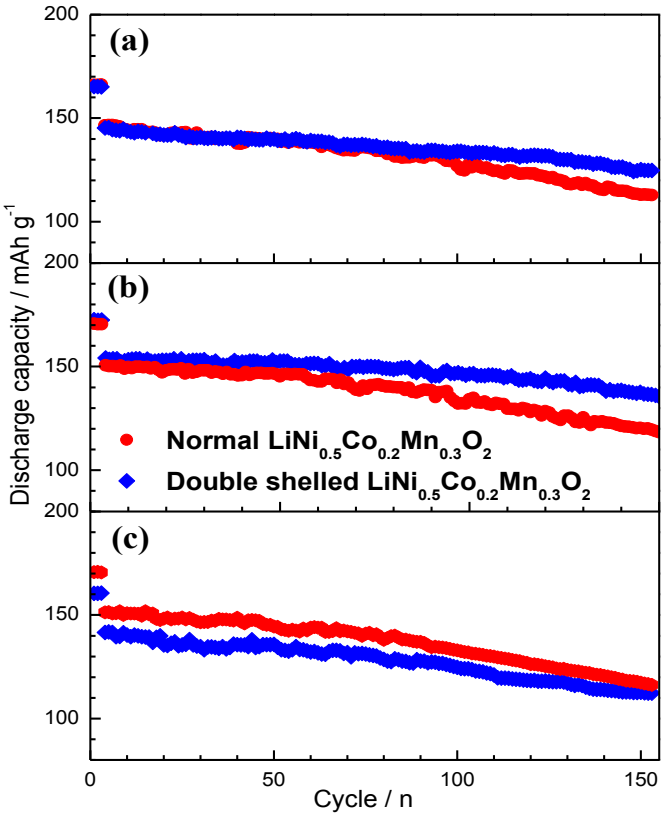

Fig. 7. Cycling performance of normal and double-shelled $LiNi_{0.5}Co_{0.2}Mn_{0.3}O_2$ calcined at different temperatures in the voltage range of 3.0–4.3 V at 25 °C at a constant current density of 20 mA g^{-1} for initial three cycles and 150 mA g^{-1} for subsequent cycles: (a) 800 °C, (b) 850 °C, (c) 900 °C.

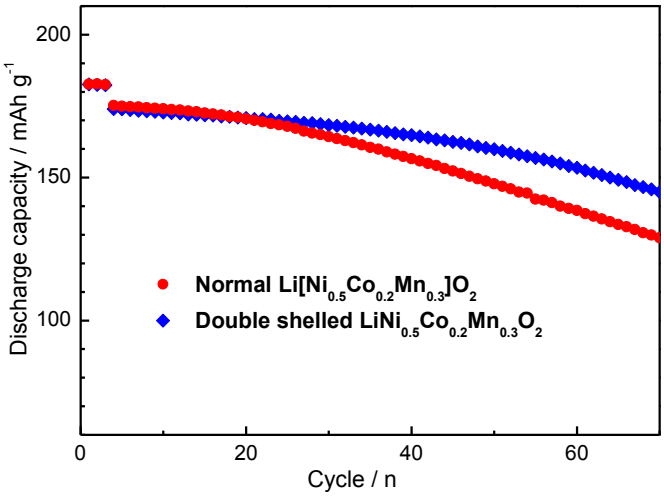

Fig. 8. Cycling performance of normal and double-shelled $LiNi_{0.5}Co_{0.2}Mn_{0.3}O_2$ prepared at 850 °C in the voltage range of 3.0–4.3 V at 55 °C at a constant current density of 20 mA g^{-1} for initial three cycles and 100 mA g^{-1} for subsequent cycles.

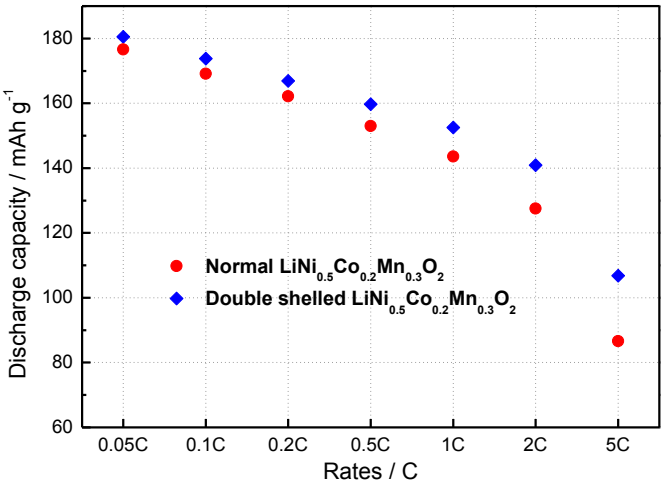

Fig. 10. The comparison in initial discharge capacity for normal and double-shelled $LiNi_{0.5}Co_{0.2}Mn_{0.3}O_2$ cycled between 3.0 and 4.3 V at 25 °C at various rates from 0.05C (8 mA g^{-1}) to 5 C (800 mA g^{-1}).

plate-like to micron-sized rectangular-like shapes. In addition, the materials with core–shell structure appears to be more porous than normal one especially prepared at 850 °C, which is also confirmed by the comparison of BET measurement that the double-shelled material prepared at 850 °C (1.26 m^2 g^{-1}) has a larger specific surface area than normal one (0.79 m^2 g^{-1}). This implies that the double-shelled sample perhaps has superior rate capability in comparison with the normal sample. The EDS analysis of double-shelled lithiated compounds of Fig. 4(a), (c) and (e) is listed in Table 3. The detected surface compositions for the double-shelled Li$[Ni_{0.5}Co_{0.2}Mn_{0.3}]O_2$ prepared at 800 °C, 850 °C and 900 °C are Li$[Ni_{0.403}Co_{0.194}Mn_{0.403}]O_2$, Li$[Ni_{0.416}Co_{0.201}Mn_{0.383}]O_2$ and Li$[Ni_{0.434}Co_{0.205}Mn_{0.361}]O_2$, respectively, indicating gradual deviation from targeted Li$[Ni_{0.4}Co_{0.2}Mn_{0.4}]O_2$ with increasing sintering temperature. It seems that the diffusion of transition metal ions between core and shell occurs and becomes severe with increasing sintering temperature. Anyhow, the EDS data can demonstrate the preservation of core–shell structure even after calcination at 900 °C; however, the shell components at a high sintering temperature possibly change somewhat, leading to a smaller compositional difference from core to shell parts.

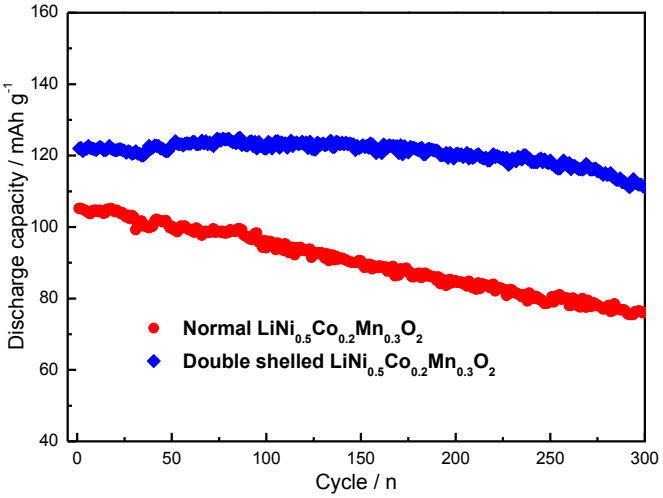

Fig. 9. Cycling life of normal and double-shelled $LiNi_{0.5}Co_{0.2}Mn_{0.3}O_2$ prepared at 850 °C at a constant current density 640 mA g^{-1} (4C) between 3.0 and 4.3 V at 25 °C.

Fig. 5 shows XRD patterns of the double-shelled and normal materials prepared at 800 °C, 850 °C and 900 °C. All materials can be indexed to a hexagonal α-$NaFeO_2$-type structure with a space group of R-3m. It is hard to find differences in XRD patterns between double-shelled and normal samples prepared at the same sintering temperature. Nevertheless, the double-shelled material displays slightly larger lattice parameters than normal one, as indicated in Table 4. In addition, the splitting between the (1 0 8) and (1 1 0) peaks becomes more clear with increasing sintering temperatures. This means that the materials prepared at a higher calcination temperature have a better-defined layered structure. The subtle changes due to different sintering temperatures can be also reflected in lattice parameters, as shown in Table 4. The lattice parameters become smaller with increasing calcination temperature.

Fig. 6 shows the initial charge–discharge curves of double-shelled and normal materials prepared at different temperatures in the voltage of 3.0–4.3 V at 25 °C at a constant current density of 20 mA g^{-1}. The initial charge–discharge capacities and columbic efficiency are summarized in Table 5. The differences in the shape of charge–discharge curves are hardly found between the core-shelled and normal samples. Nevertheless, it is found that 850 °C is the optimal sintering temperature according to these electrochemical data. Fig. 7 shows the cycling performance comparison of normal and double-shelled materials calcined at different calcination temperatures in the voltage range of 3.0–4.3 V at 25 °C at a constant current density of 20 mA g^{-1} for initial three cycles and 150 mA g^{-1} for subsequent cycle. As expected, double-shelled materials especially prepared at 850 °C exhibit much improved Li^+ intercalation stability in contrast to normal ones. The double-shelled materials prepared at 800 °C, 850 °C, and 900 °C have capacity retention of 85.95%, 87.35%, and 79.31% at 150th cycle, respectively. By contrast, the normal materials prepared at 800 °C, 850 °C, and 900 °C suffer from a severe capacity fading, leading to capacity retention of only 77.20%, 77.49% and 76.80% at 150th cycle, respectively. The significant improvement in cycleability may be possibly ascribed to $LiNi_{0.4}Co_{0.2}Mn_{0.4}O_2$ shell providing structural stability [27].

To further evaluate the effect of the core–shell structure on cycling stability of materials, electrochemical tests with the samples prepared at 850 °C were performed at an elevated temperature

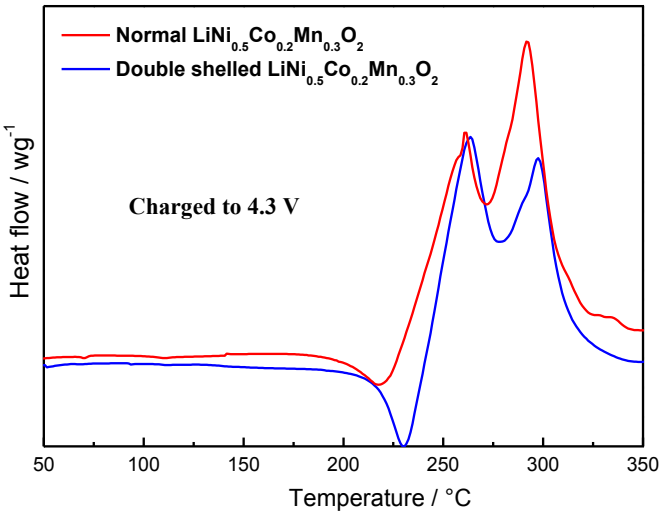

Fig. 11. DSC results of the normal and double-shelled $LiNi_{0.5}Co_{0.2}Mn_{0.3}O_2$ electrodes charged to 4.3 V.

of 55 °C in the voltage range of 3.0–4.3 V at a constant current density of 20 mA g^{-1} for initial three cycles and 100 mA g^{-1} for subsequent cycle, as shown in Fig. 8. The initial discharge capacities of the double-shelled and normal material electrodes at 55 °C increase by 10 mAh g^{-1} compared to that at 25 °C. The cycleability of double-shelled material is remarkably improved, still maintaining discharge capacity of 142.2 mAh g^{-1} (only 18.3% capacity loss) after 70 cycles. In contrast, the normal material shows a rapid decrease in capacity, leading to a capacity retention of only 72.0% (126.1 mAh g^{-1}) over the same cycling period. On the basis of the above electrochemical data, it can be concluded that construction of a suitable double-shelled core–shell structure in $LiNi_{0.5}Co_{0.2}Mn_{0.3}O_2$ can contribute to enhancing the cycleability of materials. Presumably, two factors may account for it. One factor is ascribed to structurally stable shell component of $LiNi_{04}Co_{0.2}Mn_{0.4}O_2$, which can elevate structural stability of core-shelled materials during cycling, as suggested by Sun et al. [24]. The other can be attributed to the interface between electrode materials and electrolyte. According to the report [38], the surface crystal structure of $LiNi_{0.5}Co_{0.2}Mn_{0.3}O_2$ suffers from an irreversible transformation after a large number of cycles, that is, a mixture of spinel and rock salt phases is developed on the surface of the pristine rhombohedral phase due to the highly oxidative environment that triggers the oxygen loss from the surface of the material. The presence of the ionically insulating rock salt phase may result in sluggish kinetics, thus deteriorating the capacity retention. In the double-shelled sample, a new interface based on $LiNi_{0.4}Co_{0.2}Mn_{0.4}O_2$ is constructed. $LiNi_{0.4}Co_{0.2}Mn_{0.4}O_2$ has been reported to be able to remain a simple topotactic reaction during electrochemical cycling, even at the high voltage cutoff limit of 4.6 V [27].

The cycleability comparison at a high rate of 640 mA g^{-1} (about 4C) in the voltage range of 3.0–4.3 V at 25 °C was also performed, as indicated in Fig. 9. After 300 cycles, the discharge capacity and capacity retention of the normal sample are 105.2 mAh g^{-1} and 72.4%, respectively. By contrast, the double-shelled sample displays the discharge capacity of 122.0 mAh g^{-1} and capacity retention of 90.9%. The results also show that the double-shelled sample presents better cycleability than normal sample even at a high rate. Nevertheless, a more superior reversible capacity at a high rate is observed in the double-shelled sample in contrast to normal sample. This implies that the double-shelled materials possibly have better rate performance than normal ones. The deduction is certified in Fig. 10, which shows the comparison in initial discharge capacity for normal and double-shelled $LiNi_{0.5}Co_{0.2}Mn_{0.3}O_2$ cycled between 3.0 and 4.3 V at 25 °C at various rates from 0.05C (8 mA g^{-1}) to 5C (800 mA g^{-1}). A gradually increased difference in initial discharge capacity between double-shelled and normal materials are observed with increasing rates, indicating that the double-shelled sample has better rate capability than normal one. The capacity retention ratio of 5C vs 0.05C in the double-shelled material electrode is about 59.2%, while 47.5% in normal sample. The result is possibly related to the fact that the double-shelled sample prepared at 850 °C has larger porosity than normal sample, as demonstrated from above SEM images and the BET data.

Fig. 11 shows DSC profiles of normal and double-shelled material electrodes charged to 4.3 V. The normal material electrode exhibited two exothermic peaks at 250 °C and 280 °C with a heat generation of 864 J g^{-1}. Meanwhile, double-shelled material electrode showed an improved thermal stability with two exothermic reaction at 250 °C and 290 °C and much reduced heat generation of 660 J g^{-1}. The improved thermal stability of the double-shelled material might be due to the thermally stable double shells $LiNi_{1/3}Co_{1/3}Mn_{1/3}O_2$ and $LiNi_{0.4}Co_{0.2}Mn_{0.4}O_2$, which can suppress oxygen release from the host lattice.

4. Conclusion

A new double-shelled $Li[(Ni_{0.8}Co_{0.1}Mn_{0.1})_{2/7}]_{core}[(Ni_{1/3}Co_{1/3}Mn_{1/3})_{3/14}]_{inner\text{-}shell}[(Ni_{0.4}Co_{0.2}Mn_{0.4})_{1/2}]_{outer\text{-}shell}O_2$ structure was proposed to improve battery performances of $LiNi_{0.5}Co_{0.2}Mn_{0.3}O_2$ and achieved successfully from corresponding core-shelled precursors obtained via a co-precipitation route. Increase of particles size of hydroxide precursors from core to shell, in combination with the investigations of EDS, SEM and ICP on precursors and lithiated compounds, demonstrates the formation of the core-shelled structure. However, sintering temperature for preparation of lithiated compounds has great impacts on morphology, structure, cation diffusion in core-shelled structure and electrochemical performances. It seems that 850 °C is an optimal sintering temperature according to electrochemical performances. Consequently, the double-shelled $LiNi_{0.5}Co_{0.2}Mn_{0.3}O_2$ presents remarkably improved cycling performance, thermal stability, and rate capability in contrast to normal $LiNi_{0.5}Co_{0.2}Mn_{0.3}O_2$, which might be due to the double shells providing structural and thermal stability or better interface between electrode and electrolyte. Additionally, the concept of designing $LiNi_{0.5}Co_{0.2}Mn_{0.3}O_2$ into new double-shelled or multi-shelled structure with the aid of the triangle phase diagram of $LiNiO_2$–$LiCoO_2$–$LiMnO_2$ is instructive in searching for new improved cathode materials.

Acknowledgments

This work was financially supported partly by National 863 Program of China (2011AA11A234, 2013AA050906), National Natural Science Foundation of China (51272175, 20901058, 21301127) and Program for New Century Excellent Talents in University of China (NCET-10-0952).

References

[1] J.M. Tarascon, M. Armand, Nature 414 (2001) 359.
[2] Z. Lu, D.D. MacNeil, J.R. Dahn, Electrochem. Solid-State Lett. 4 (2001) 200.
[3] D. MacNeil, Z. Lu, J.R. Dahn, J. Electrochem. Soc. 149 (2002) 1332.
[4] S. Jouanneau, D.D. Macneil, J.R. Dahn, J. Electrochem. Soc. 150 (2003) 1299.
[5] S. Jouanneau, K.W. Eberman, J.R. Dahn, J. Electrochem. Soc. 150 (2003) 1637.
[6] T. Ohzuku, Y. Makimura, Chem. Lett. 7 (2001) 642.
[7] J.K. Ngala, N.A. Chernova, M.S. Whittingham, J. Mater. Chem. 14 (2004) 214.
[8] P. Li, E.S. Han, B.S. Tan, Chin. J. Appl. Chem. 22 (2005) 304.
[9] S.H. Kang, J. Kim, M.E. Stoll, J. Power Sources 112 (2002) 41.

[10] J. Choi, A. Manthiram, J. Power Sources 162 (2006) 667.
[11] H. Cao, Y. Zhang, J. Zhang, Solid State Ionics 176 (2005) 1207.
[12] Y.C. Su, W. Xie, P. Yu, Mater. Sci. Eng. Powder Metall. 10 (2005) 149.
[13] M.H. Kim, H.S. Shin, D.W. Shin, Y.K. Sun, J. Power Sources 159 (2006) 1328.
[14] D. Li, Y. Sasaki, M. Kageyama, K. Kobayakawa, Y. Sato, J. Power Sources 148 (2005) 85.
[15] S. Lee, D. Jang, J. Yoon, Y.H. Cho, Y.S. Lee, D.H. Kim, W.S. Kim, W.S. Yoon, J. Electrochem. Sci. Technol. 3 (2012) 29.
[16] S.B. Kim, K.J. Lee, W.J. Choi, W.S. Kim, I.C. Jang, H.H. Lim, Y.S. Lee, J. Solid State Electrochem. 14 (2012) 919.
[17] Y.H. Cho, D. Jang, J. Yoon, H. Kim, T.K. Ahn, K.W. Nam, Y.E. Sung, W.S. Kim, Y.S. Lee, X.Q. Yang, W.S. Yoon, J. Alloys Compd. 562 (2013) 219.
[18] F. Wang, Y. Zhang, J.Z. Zou, W.J. Liu, Y.P. Chen, J. Alloys Compd. 558 (2013) 172.
[19] J.Z. Kong, F. Zhou, C.B. Wang, X.Y. Yang, H.F. Zhai, H. Li, J.X. Li, Z. Tang, S.Q. Zhang, J. Alloys Compd. 554 (2013) 221.
[20] K. Yang, L.Z. Fan, J. Guo, X.H. Qu, Electrochim. Acta 63 (2012) 363.
[21] W. Liu, M. Wang, X.L. Gao, W.D. Zhang, J.T. Chen, H.H. Zhou, J. Alloys Compd. 543 (2012) 181.
[22] Y.S. Bai, X.Y. Wang, S.Y. Yang, X.Y. Zhang, X.K. Yang, H.B. Shu, Q. Wu, J. Alloys Compd. 541 (2012) 125.
[23] P.Y. Hou, J. Guo, D.W. Song, J. Zhang, E.L. Zhou, L.Q. Zhang, Chem. Lett. 41 (2012) 1712.
[24] Y.K. Sun, S.T. Myung, M.H. Kim, J. Prakash, K. Amine, J. Am. Chem. Soc. 127 (2005) 13411.
[25] X.K. Yang, X.Y. Wang, G.S. Zou, L. Hu, H.B. Shu, S.Y. Yang, L. Liu, H. Hu, H. Yuan, B.N. Hu, Q.L. Wei, L.H. Yi, J. Power Sources 232 (2013) 338.
[26] X.K. Yang, X.Y. Wang, L. Liu, G.S. Zou, S.J. Su, Y.S. Bai, H.B. Shu, Q.L. Wei, B.N. Hu, L. Ge, D. Wang, L. Liu, Hu, J. Power Sources 242 (2013) 589.
[27] K.S. Lee, S.T. Myung, Y.K. Sun, Chem. Mater. 19 (2007) 2727.
[28] W.S. Yoon, Y. Paik, X.Q. Yang, M. Balasubramanian, J. McBreen, C.P. Grey, Solid State Lett. 5 (2002) 263.
[29] S.Y. Yang, X.Y. Wang, X.K. Yang, Z.L. Liu, Y.S. Bai, H.B. Shu, J. Solid State Electrochem. 16 (2012) 2823.
[30] S.T. Myung, K. Izumi, S. Komaba, H. Yashiro, H.J. Bang, Y.K. Sun, N. Kumagai, J. Phys. Chem. C 111 (2007) 4061.
[31] W.B. Luo, X.H. Li, J.R. Dahn, Chem. Mater. 22 (2010) 5065.
[32] X.Q. Yang, J. McBreen, W.S. Yoon, C.P. Grey, Electrochem. Commun. 4 (2002) 649.
[33] S.T. Myung, S. Komaba, K. Hosoya, N. Hirosaki, U. Miura, N. Kumagai, Chem. Mater. 17 (2005) 2427.
[34] Z. Lu, L.Y. Beaulieu, R.A. Donaberger, C.L. .Thomas, J.R. Dahn, J. Electrochem. Soc. 149 (2002) 778.
[35] L.Q. Zhang, C.W. Xiao, R.J. Yang, Prog. Chem. 23 (2011) 410.
[36] Y.K. Sun, S.T. Myung, B.C. Park, J. Prakash, I. Belharouak, K. Amine, Nat. Mater. 8 (2009) 320.
[37] H. Shi, X.Q. Wang, P.Y. Hou, E.L. Zhou, J. Guo, J. Zhang, D.G. Wang, F.X. Guo, D.W. Song, X.X. Shi, L.Q. Zhang, J. Alloys Compd. 587 (2014) 710.
[38] S.K. Jung, H. Gwon, J. Hong, K.Y. Park, D.H. Seo, H. Kim, J. Hyun, W. Yang, K. Kang, Adv. Energy Mater. 4 (2014) 1300787.